

RESEARCH LETTER

10.1002/2014GL062571

Key Points:

- Relative merits of finite-frequency tomography versus ray theory approach
- Models independent validation by full waveform propagation and statistics
- Finite-frequency images are superior for certain regions

Supporting Information:

- Readme
- Figure S1
- Figure S2
- Figure S3
- Figure S4
- Figure S5

Correspondence to:

M. Maceira,
mmaceira@lanl.gov

Citation:

Maceira, M., C. Larmat, R. W. Porritt, D. M. Higdon, C. A. Rowe, and R. M. Allen (2015), On the validation of seismic imaging methods: Finite frequency or ray theory?, *Geophys. Res. Lett.*, 42, 323–330, doi:10.1002/2014GL062571.

Received 19 NOV 2014

Accepted 27 DEC 2014

Accepted article online 6 JAN 2015

Published online 23 JAN 2015

On the validation of seismic imaging methods: Finite frequency or ray theory?

Monica Maceira¹, Carene Larmat¹, Robert W. Porritt^{2,3}, David M. Higdon¹, Charlotte A. Rowe¹, and Richard M. Allen³

¹Earth and Environmental Sciences Division, Los Alamos National Laboratory, Los Alamos, New Mexico, USA,

²Department of Earth Sciences, University of Southern California, Los Angeles, California, USA, ³Department of Earth and Planetary Science, University of California, Berkeley, California, USA

Abstract We investigate the merits of the more recently developed finite-frequency approach to tomography against the more traditional and approximate ray theoretical approach for state of the art seismic models developed for western North America. To this end, we employ the spectral element method to assess the agreement between observations on real data and measurements made on synthetic seismograms predicted by the models under consideration. We check for phase delay agreement as well as waveform cross-correlation values. Based on statistical analyses on *S* wave phase delay measurements, finite frequency shows an improvement over ray theory. Random sampling using cross-correlation values identifies regions where synthetic seismograms computed with ray theory and finite-frequency models differ the most. Our study suggests that finite-frequency approaches to seismic imaging exhibit measurable improvement for pronounced low-velocity anomalies such as mantle plumes.

1. Introduction

When an earthquake or an underground explosion occurs, the seismic waves that are generated propagate through the Earth, sensing its three-dimensional structure. The waveforms recorded for many events at many stations around the world can be used to image the structure using tomographic approaches. Since the beginning of tomography studies in the 1970s [Aki *et al.*, 1977; Sengupta and Toksöz, 1977; Dziewonski *et al.*, 1977], geoscientists have furthered the art of inferring an image of the underground solid Earth from a collection of observables recorded at the surface. While recent developments in tomography methods, together with vastly increased density of sensors, have led to unprecedented resolution of 3-D seismic models, they do not generally provide an assessment of the model uncertainty. Model validation is typically limited to resolution tests, which only consider the impact of the data coverage on resolution [e.g., Menke, 1989; Lévêque *et al.*, 1993; Fichtner and Trampert, 2011], by assuming that the imaging theory itself is accurate. In a time when decision makers use these models for economic and societal needs [Showstack, 2014], and researchers around the world develop competing Earth models, there is a need to validate and quantify the uncertainties of 3-D geophysical models [Ma *et al.*, 2008; Bozdog and Trampert, 2010; Maceira *et al.*, 2011; Larmat *et al.*, 2011; Gao and Shen, 2012].

Motivated by the large number of disparate models recently published and thanks to past decades' advances in computational power, as well as improved instrumentation and coverage, we validate state of the art seismic models developed for western North America. We are also able to independently assess crucial aspects of tomographic imaging with matrix inversions in relation to their data via the Spectral Element Method (SEM) [Komatitsch and Vilotte, 1998; Komatitsch *et al.*, 2002]. We investigate the relative benefits of finite-frequency (FF) tomography [e.g., Marquering *et al.*, 1999; Dahlen *et al.*, 2000; Hung *et al.*, 2000] compared to the traditional and more approximate ray theoretical (RT) approach. Although FF provides a better forward theory to represent the wavefield [Hung *et al.*, 2001], debate continues as to whether its application to tomography produces better models. Much of the literature concerned with the topic focuses on surface waves, and while numerous studies report improved tomographic images [e.g., Peter *et al.*, 2009, and references therein], others [e.g., Boschi *et al.*, 2006, and references therein] suggest that theoretical advances of FF may be outweighed by practical considerations and that RT models are indistinguishable from FF when realistic ray coverage and noise are considered. When focusing on body wave imaging, numerical experiments by Mercerat *et al.* [2014] and Liu *et al.* [2009] showed that FF can

achieve more accurate inversion results than RT. Experiments by *Spetzler et al.* [2007] concluded that both imaging methods can produce satisfactory results if the imaged structure is comparable in size to the Fresnel zone, but only FF is satisfactory for smaller structures. On a global scale, numerical simulations by *Hwang et al.* [2011] showed that narrow mantle plumes cannot be resolved by FF at seismic periods commonly used. This conclusion contradicts the resolution analysis for many plumes imaged by *Montelli et al.* [2004a, 2006] using a FF approach.

In this paper, we test this limit through direct comparison of FF and RT models making use of Los Alamos National Laboratory (LANL) high-performance computational (HPC) resources that allow us to test and verify models through full three-dimensional waveform modeling using SEM. First, we introduce the reader to the Dynamic North America (DNA09) models and our approach to model validation via the SEM. We continue with a description of the analyses performed on the synthetic seismograms to conclude with our findings about the merits of finite-frequency imaging methods. Implementation of the method for a densely instrumented region such as that covered by the DNA09 models provides a useful test bed for the validation methods that we will later apply to other study areas. These regions are less well instrumented but are of interest to more confidently and accurately locate events of interest for nuclear monitoring.

2. The Model and the Validation Set

Recent theoretical developments in seismic wave propagation now provide the basis for a new generation of seismic models. In addition, seismic waveform data sets from dense continental-scale deployments (e.g., USArray [*Long et al.*, 2014]) are now available, providing the opportunity to apply FF tomography on a regional or continental scale and compare the results with traditional RT models for the same regions. Here we focus on validation of the Dynamic North America (DNA09) models developed using both the body-wave FF approach [*Obrebski et al.*, 2010; *Xue and Allen*, 2010] and the RT approach (generated also by the Berkeley group for this study). There are many other models that could be used in such a validation study. In choosing the DNA09 models, we can undertake a realistic study (in contrast with numerical and synthetic works [e.g., *Mercurat et al.*, 2014]) and limit the vast parameter space within which seismic models can be generated. Both FF and RT models used here were computed with the same data selection and processing as well as the same reference model, all of which were pointed out by *Becker* [2012] to have a large effect on the final model. This was confirmed by *Auer et al.* [2014] who showed that tomographic models could exhibit large differences.

The DNA09 models are derived from relative delay times compared to iasp91 [*Kennett and Engdahl*, 1991] of body waves (direct *P*, direct *S*, and *SKS*) recorded with the USArray. The arrival time windows are hand picked, and the delays are refined via the multichannel cross correlation of *VanDecar and Crosson* [1990]. These delays are accumulated along a raypath, which is used to populate the inversion matrix. The inverse problem is then solved with standard least squares regression using damping and smoothing regularization to stabilize the solution. Additionally, event and station static corrections are solved for in order to account for small errors in the timing and location of the events and to absorb the structure of the upper 100 km where teleseismic raypaths do not cross before reaching the station. The differences between the RT and FF models are manifested in the inversion matrix. In the RT case, the sensitivity is evenly distributed along the center of the ray to the resolution limit of the grid cells. The FF model uses the single scatterer (Born) approximation to calculate the frequency-dependent sensitivity along the raypath, which vanishes at the center and has a sinusoidal cross section extending to approximately the square root of the dominant wavelength from the center. Due to this inherently smooth sensitivity kernel, the FF inversion does not use smoothing regularization. Visual inspection of the resulting FF and RT models at different depths shows the same features at long wavelength with some discrepancies for the shortest wavelengths (comparisons are included in the supporting information), and histograms of the differences between the two models fit zero-centered Gaussian functions. These differences, although small, should be studied and interpreted in terms of merits of the imaging methods.

We choose a validation set consisting of 14 seismic events of different types and magnitudes with broad azimuthal coverage (Table 1 and supporting information). For each event, we compute synthetic seismograms through both the FF and RT DNA09 models using the SEM (see examples in the supporting information). This allows independent forward calculations through a full 3-D model. The SEM makes no assumptions about the theory used to generate the models, but it requires substantial computational

Table 1. List of Earthquakes Used for Validation With Their Coordinates, Magnitude, Backazimuth to Yellowstone and Their Respective Number of *S* Phase Delay Time Measurements for *SV* and *SH*

<i>i</i>	Date	Latitude	Longitude	Depth (km)	Magnitude	Backazimuth (to Yellowstone)	n_{SV}	n_{SH}
1	2007-02-12	35.90	349.70	44.8	6.0	56.3	145	113
2	2007-04-05	37.45	335.56	12.0	6.3	63.2	128	286
3	2007-08-20	8.19	320.83	12.0	6.5	96.3	408	219
4	2008-02-08	10.85	318.29	16.8	6.9	96.2	252	276
5	2008-05-23	7.51	324.99	12.6	6.5	93.7	401	63
6	2008-09-10	8.18	321.46	15.3	6.6	95.8	461	331
7	2007-11-18	-22.67	293.52	262.4	6.0	137.0	53	265
8	2007-01-13	46.17	154.80	12.0	8.1	306.8	278	334
9	2007-12-13	-15.24	188.03	21.3	6.2	237.0	275	53
10	2007-12-19	51.02	180.73	27.6	7.1	301.5	445	467
11	2008-11-24	54.27	154.71	502.2	7.3	314.7	344	543
12	2007-10-31	18.83	145.59	210.9	7.2	291.2	123	122
13	2007-11-14	-22.64	289.38	37.6	7.7	140.8	361	367
14	2008-02-14	36.24	21.79	20.0	6.8	35.2	0	0

resources. The SEM solves the wave equation in its integral form on meshes made of hexahedral elements built from the cubed sphere and honoring major seismic discontinuities. It employs a high-order finite element method with exponential convergence for smooth solutions while maintaining the geometric flexibility of finite elements [Komatitsch and Vilotte, 1998; Komatitsch and Tromp, 2002]. We use the modeling package SPECFEM3D [Komatitsch et al., 2002]. We compare the synthetics at 1061 stations generated through both the FF and RT models as well as with real seismograms observed at those stations for the selected events. We analyze *S* phase delay measurements—with respect to iasp91—and waveform correlation for comparison.

3. Analysis and Results

3.1. Phase Delay Analysis

To assess the quality of the RT and FF models, we treated synthetic seismograms in the same way as the real observations and measured *S* wave (*SH* and *SV*) phase delays on the synthetic seismograms following the same methodology that was used to measure phase delays for the generation of the DNA09 models. We rotated the data from the Vertical-North-East coordinate frame into the *P-SV-SH* coordinate frame using TauP [Crotwell et al., 1999] to compute the slowness parameter for the model. Preliminary tests have shown that the *P* model synthetics lack sufficient high-frequency content to properly replicate the observations (synthetics are accurately computed down to 10 s) and thus are not used in the following procedure. Direct *SV* and *SH* arrivals were handpicked independently on the synthetics from the RT and FF models. Because we are using relative arrival times, the observed delays depend on the set of stations being correlated. The synthetic picks were, therefore, joined with the set of stations having acceptable picks for the real data and multichannel cross correlation was repeated for the synthetic and real data sets. We then compared the observed delay times from the real data with the measured delay times from each of the synthetic data sets. In a complete match, the synthetic delays would be the same as the real delay. We can then determine the quality of the model by assessing the misfit between the real and synthetic delay (Figure 1). From Figure 1 it is clear that the time delays produced by the two models are more similar to one another than they are to the actual delays. The mean absolute residuals between the actual and model-based delay times are shown in Figure 2. Clearly the ability of the models to reproduce the actual delay times varies from event to event. Both RT and FF models do a poor job with events 8 and 10, while the results for events 4, 6, and 12 are much more in line with the actual observations. From events 3–6, 8, and 9, it is apparent that the models have difficulty reproducing the small actual delays present in the northern stations given by the blue, purple, and black pixels of the first column of Figure 1. The models do better reproducing the large delays given by the light/yellow pixels in the figure. On average, the delay times produced by the FF model are 0.07 s closer to the actual delay times for *SV* and 0.03 s closer for *SH*. A simple paired *t* test [Box et al., 1978] can

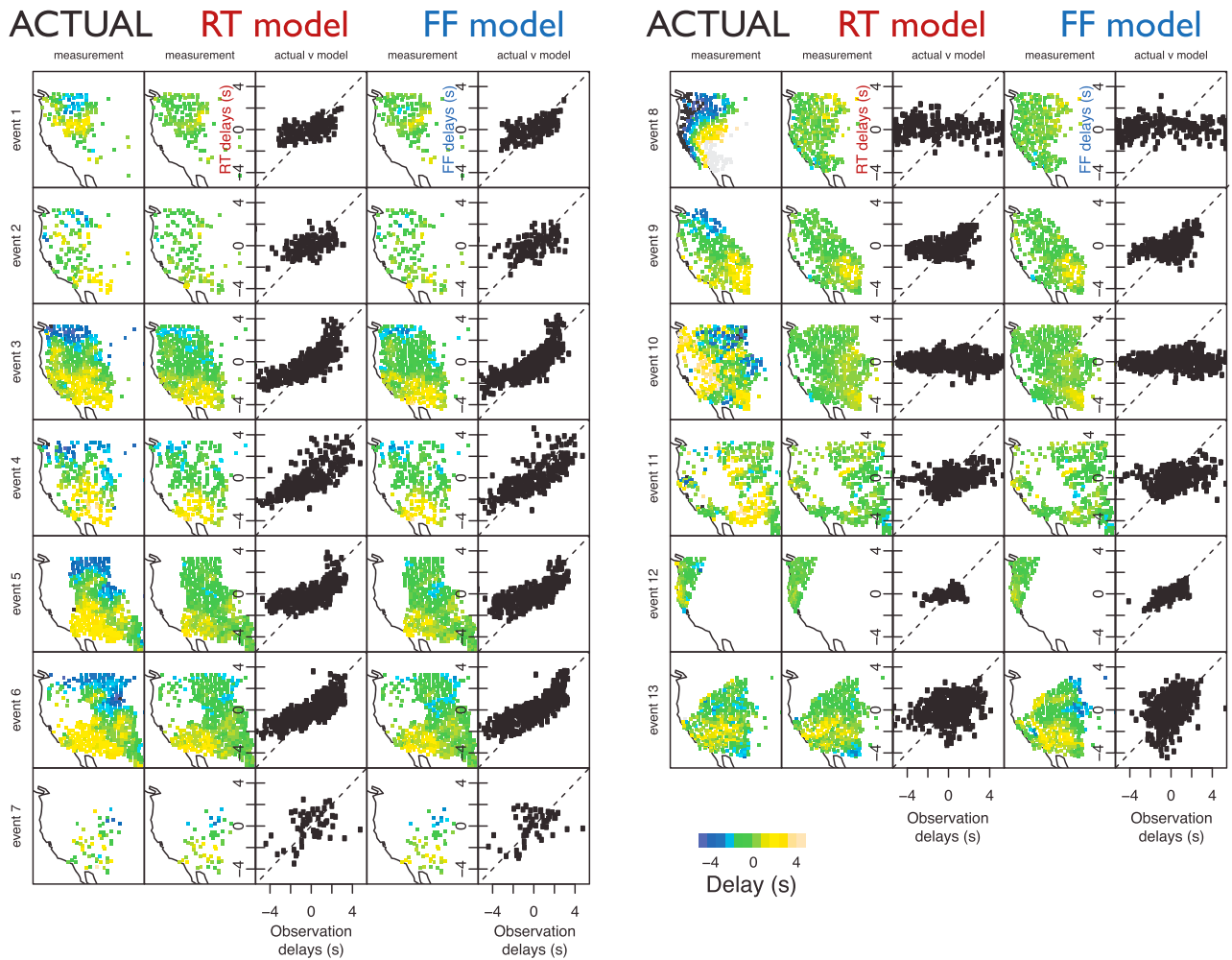


Figure 1. A comparison of actual and modeled SV delay times (with respect to model iasp91). The plots show the actual and modeled measurements at their spatial locations as well as actual measured arrival times (x axis) plotted against the modeled arrival times (y axis).

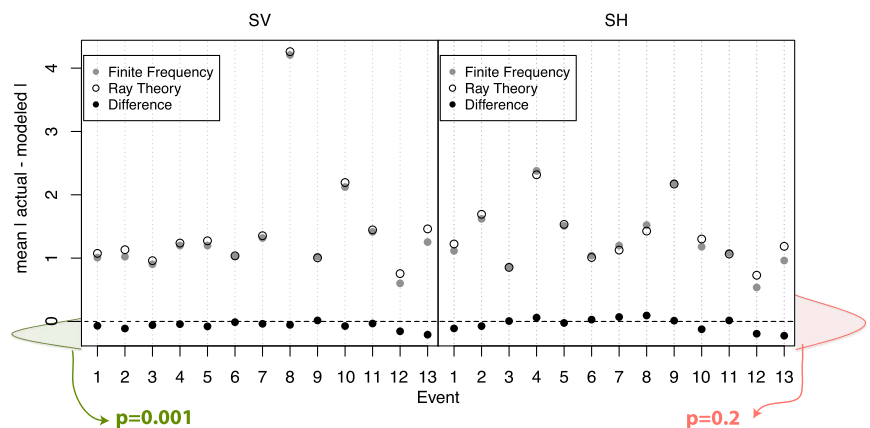


Figure 2. For each station measurement, the misfit between observed and modeled delay times—with respect to iasp91—is summarized by the mean of the absolute deviations. The differences resulting from each pair of models for the 13 events are given by the black dots. The difference is statistically significant, favoring smaller absolute SV residuals for the FF model (schematically represented by the narrower green distribution shifted away from zero). There is no significant difference in mean absolute residuals for the SH delay times (wider and more zero centered red distribution).

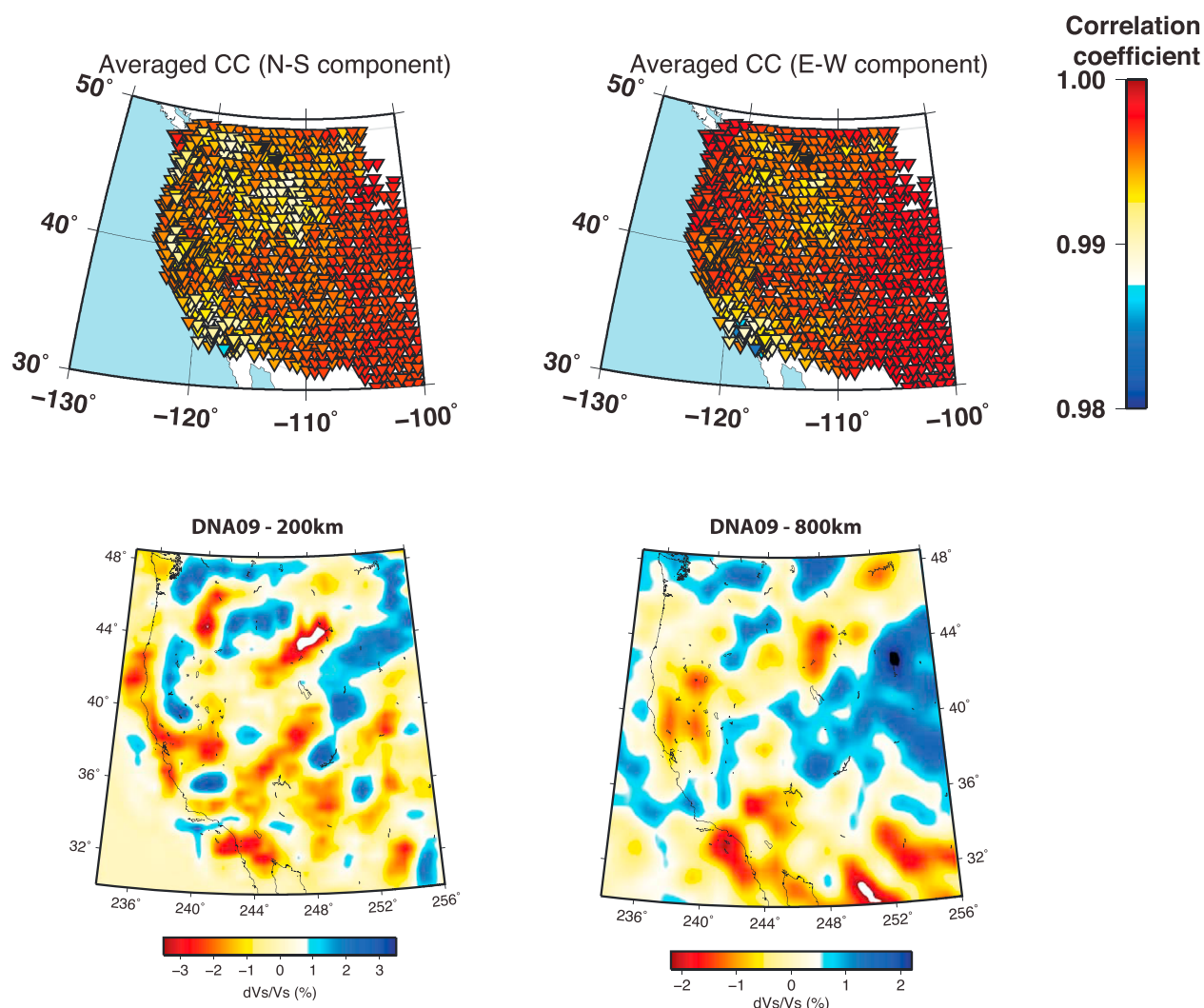


Figure 3. (top) Waveform cross-correlation coefficients between FF and RT horizontal components synthetics for each station are averaged for all 14 events in our study. (bottom) FF DNA09 model depth slices at (left) 200 km and (right) 800 km (right).

be used to assess the significance of this observed difference. The difference is significant for the *SV* arrival times ($p = 0.001$) and not for the *SH* arrival times ($p = 0.2$). These differences are shown graphically by the black dots in Figure 2. Based on *S* wave phase delay measurements, the models are statistically different and FF DNA09 performs better than the RT DNA09 model for *SV* measurements, but there is no significant difference between the two models for *SH* measurements.

3.2. Cross-Correlation Analysis

Focusing on only the *S* phase and proceeding in the same manner as applied to the real observations, we filtered the synthetic seismograms in a passband between 10 and 50 s and computed waveform cross-correlation coefficients between RT and FF synthetics for a 55 s window around the *S* phase. We then averaged the resulting cross-correlation coefficients between the horizontal components of RT and FF synthetic seismograms for all 14 events and for each of the 1061 stations. We computed statistics under various norms (median, variance, L1, and L2), and all lead to the same conclusion; thus, we present here only results for the mean in Figure 3 (top). Coefficient values show that the synthetics for the time window around the *S* phase are nearly identical for FF and RT models, except for stations located near Yellowstone, and in the southwestern corner of the model. Careful scrutiny of the model images for these two regions (Figure 3 (bottom)) indicates an association between these stations and low-velocity anomalies in the seismic model, suggesting that FF better illuminates large-amplitude, low-velocity features such as mantle plumes [Montelli *et al.*, 2004a]. This contradicts Hwang *et al.* [2011] who, based on numerical simulations,

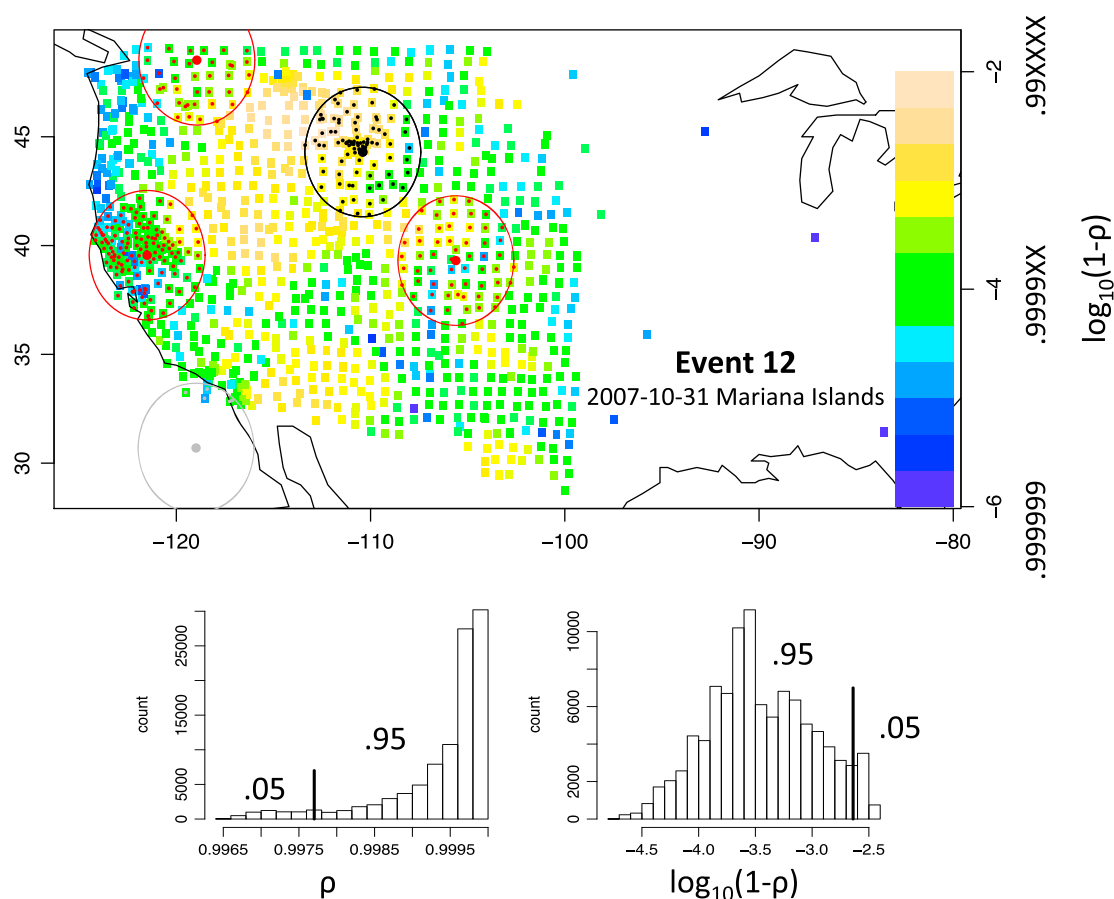


Figure 4. (top) Permutation test for waveform cross-correlation coefficients for stations around Yellowstone for event 12 in our validation data set. (bottom) Histograms of cross correlations from 100,000 random locations indicate the Yellowstone region resides at about the 5th percentile ($p = 0.05$) of these 100,000 realizations.

concluded that narrow lower mantle plumes are seismically invisible. The contradiction is probably caused by Hwang et al. placing the plume at the antipode to facilitate the computations, thus making it always in the doughnut hole. This, in addition to the plume being thin enough to be covered by the doughnut hole, makes it disappear in seismograms from stations at a short distance from the plume.

To test the statistical significance of cross-correlation differences between Yellowstone and other regions, we applied a spatial randomization test [Manly, 2007] to determine if the cross correlations between FF and RT synthetics near Yellowstone are, on average, smaller than the average cross correlation of stations near a randomly chosen location. The basic elements of this randomization test are the following:

1. The test statistic: the mean of the cross-correlation coefficients for all stations within a 300 km radius of the location.
2. The null hypothesis: the Yellowstone location is not different from any randomly chosen location in the western U.S.
3. The comparison of the test statistic for the Yellowstone location to the distribution of the test statistic under the null hypothesis. The test statistics computed at 100,000 randomly chosen locations are used to sample this distribution.

An example of the analysis is shown in Figure 4 for event 12. We take the average coefficient value over all stations within a 300 km radius of Yellowstone (black circle) and compare it with cross-correlation coefficient averages for stations within 300 km of randomly chosen locations over the spatial region (red circles). We only considered circle locations that contained at least 10 stations. We generated 100,000 randomly chosen locations, comparing the average coefficient to the Yellowstone-centered average. The rank (from smallest to largest) of the Yellowstone average over 100,001 gives the one-sided p value for this test.

The permutation test demonstrates that for event 12, stations within 300 km of Yellowstone lie in the 5th percentile ($p = 0.05$) of these 100,000 realizations, which is a robust determination of significance for the difference between FF and RT synthetic seismograms. Repeating the analysis for all events, we observe an azimuthal dependence: for events 9–12, all of which occurred to the west, Yellowstone stands out as a statistically significant anomaly, whereas the remaining events do not exhibit this anomaly.

4. Conclusions

While modern inversion methods are providing unprecedented resolution for 3-D seismic structure models, there remains a lack of meticulous validation and uncertainty assessment in 3-D Earth imaging. Here we validate state of the art seismic models developed for western North America (DNA09 models) and we investigate the relative merits of the FF versus RT tomographic techniques. We use SEM to generate synthetic seismograms from 14 earthquakes, at 1061 stations across the western USA, and we statistically assess their significance and differences. Statistical analyses of *S* wave phase delay measurements, and comparison of waveform cross-correlation coefficients between FF and RT synthetics, indicate that the images generated through FF tomography are superior to those generated through RT. This advantage, however, appears to be restricted to regions possessing pronounced low-velocity anomalies such as mantle plumes. This conclusion is in good agreement with findings by *Montelli et al.* [2004b]. We do not see statistically significant differences for fast regions (e.g., subducting slabs) as *Obayashi et al.* [2013] pointed out. This could be due to an asymmetry in fast/slow anomaly size [*Hung et al.*, 2001], but we do not have an extreme early arrival through our models to test the possibility.

We questioned whether regularization choices made in the case of the RT and DNA09 parameterization did not take full advantage of the finite-frequency kernel sensitivity [*Zaroli et al.*, 2010]. To test this idea, we computed a RT DNA09 model in which we changed the regularization such that the final model has the same forward misfit as the FF DNA09 model. The results of the statistical analyses were the same. We then studied the effect of the model parameterization against the RT or FF models by extracting a single ray/kernel from the sensitivity matrix of DNA09 (see supporting information). We forced no interpolation/extrapolation so as to only view the normalized sensitivity as it is used in the inversion. In the case of a very fine mesh, the FF kernels demonstrate that there is no sensitivity along the RT path. In the case of a very coarse mesh, the FF kernels are undersampled, and thus, the improvement is small. The DNA09 grid, parameterized on nodes of $0.45313^\circ \times 0.45313^\circ \times 39.06250$ km (longitude \times latitude \times depth), is fine enough that the FF kernels provide an improved sensitivity matrix over the RT approximation.

Mercerat et al. [2014] clearly showed that the extra resolution of FF approaches to tomography originates from the use of multiple frequencies. The compressional DNA09-P FF model uses traveltimes measurements from four different frequency bands (0.02–0.1, 0.1–0.4, 0.4–0.8, and 0.8–2 Hz), in contrast with the DNA09-S model for which only the 0.02–0.1 Hz frequency band was found to have sufficiently high signal-to-noise ratio. We thus postulate that the use of a single low-frequency band in the generation of the shear wave DNA09-S model might have precluded larger differences between both seismic imaging methods.

References

- Aki, K., A. Christofferson, and E. S. Husebye (1977), Determination of the three-dimensional seismic structure of the lithosphere, *J. Geophys. Res.*, *82*, 277–296.
- Auer, L., L. Boschi, T. W. Becker, T. Nissen-Meyer, and D. Giardini (2014), Savani: A variable resolution whole-mantle model of anisotropic shear velocity variations based on multiple data sets, *J. Geophys. Res. Solid Earth*, *119*, 3006–3034, doi:10.1002/2013JB010773.
- Becker, T. W. (2012), On recent seismic tomography for the western United States, *Geochem. Geophys. Geosyst.*, *13*, Q01W10, doi:10.1029/2011GC003977.
- Boschi, L., T. W. Becker, G. Soldati, and A. M. Dziewonski (2006), On the relevance of Born theory in global seismic tomography, *Geophys. Res. Lett.*, *33*, L06302, doi:10.1029/2005GL025063.
- Box, G. E., W. G. Hunter, and J. S. Hunter (1978), *Statistics for Experimenters: An Introduction to Design, Data Analysis, and Model Building*, Wiley Series in Probability and Statistics, Wiley, New York.
- Bozdog, E., and J. Trampert (2010), Assessment of tomographic mantle models using spectral element seismograms, *Geophys. J. Int.*, *180*(3), 1187–1199.
- Crotwell, H. P., T. J. Owens, and J. Ritsema (1999), The TauP toolkit: Flexible seismic travel-time and ray-path utilities, *Seismol. Res. Lett.*, *70*, 154–160.
- Dahlen, F. A., S.-H. Hung, and G. Nolet (2000), Fréchet kernels for finite-frequency traveltimes—I. Theory, *Geophys. J. Int.*, *141*, 157–174.
- Dziewonski, A. M., B. H. Hager, and R. J. O'Connell (1977), Large-scale heterogeneities in the lower mantle, *J. Geophys. Res.*, *82*(2), 239–255, doi:10.1029/JB082i002p00239.

Acknowledgments

Thanks to Guust Nolet and Tarje Nissen-Meyer for their thoughtful reviews that considerably improved the original manuscript. We thank Peter Loxley and Yasuyuki Kato for providing useful discussion regarding the use of statistics for the purpose of models validation. Special thanks to the Data Management Center of IRIS for making the data so easily accessible to us (data from II, IU, TA, and U.S. networks were used in this study), to CI-G for developing and facilitating software, and to LANL Institutional Computing Program for providing HPC resources. We thank *Wessel and Smith* [1991], the developers of the Generic Mapping Tools software, which we use to create many of the illustrations of our research. This work was performed under the auspices of the U.S. Department of Energy by Los Alamos National Laboratory under contract DE-AC52-06NA25396/LA12-SignalPropagation-NDD2AB and grant ID 116467 under research program LFRP-Lab Fees.

The Editor thanks Guust Nolet and Tarje Nissen-Meyer for their assistance in evaluating this paper.

- Fichtner, A., and J. Trampert (2011), Hessian kernels of seismic data functionals based upon adjoint techniques, *Geophys. J. Int.*, *185*, 775–798, doi:10.1111/j.1365-246X.2011.04966.x.
- Gao, H., and Y. Shen (2012), Validation of shear-wave velocity models of the Pacific Northwest, *Bull. Seismol. Soc. Am.*, *102*(6), 2611–2621, doi:10.1785/0120110336.
- Hung, S.-H., F. A. Dahlen, and G. Nolet (2000), Fréchet kernels for finite-frequency traveltimes—II. Examples, *Geophys. J. Int.*, *141*, 175–203.
- Hung, S.-H., F. A. Dahlen, and G. Nolet (2001), Wavefront healing: A banana-doughnut perspective, *Geophys. J. Int.*, *146*, 289–312.
- Hwang, Y. K., J. Ritsema, P. E. van Keken, S. Goes, and S. Elinor (2011), Wavefront healing renders deep plumes seismically invisible, *Geophys. J. Int.*, *187*, 273–277, doi:10.1111/j.1365-246X.2011.05173.x.
- Kennett, B. L. N., and E. R. Engdahl (1991), Travel times for global earthquake location and phase association, *Geophys. J. Int.*, *105*, 429–465.
- Komatitsch, D., and J. Tromp (2002), Spectral-element simulations of global seismic wave propagation: II. Three-dimensional models, oceans, rotation and self-gravitation, *Geophys. J. Int.*, *150*, 303–318.
- Komatitsch, D., and J.-P. Vilotte (1998), The spectral element method: An effective tool to simulate the seismic response of 2D and 3D geological structures, *Bull. Seism. Soc. Am.*, *88*, 368–392.
- Komatitsch, D., J. Ritsema, and J. Tromp (2002), The spectral-element method, Beowulf computing, and global seismology, *Science*, *298*(5599), 1737–1742.
- Larmat, C., M. Maceira, and C. A. Rowe (2011), Validating 3D seismic velocity models using the spectral element method, *Seismol. Res. Lett.*, *82*(2), 280.
- Lévêque, J. J., L. Rivera, and G. Wittlinger (1993), On the use of the checkerboard test to assess the resolution of tomographic inversions, *Geophys. J. Int.*, *115*, 313–318.
- Liu, Y., L. Dong, Y. Wang, J. Zhu, and Z. Ma (2009), Sensitivity kernels for seismic Fresnel volume tomography, *Geophys.*, *74*(5), U35–U46, doi:10.1190/1.3169600.
- Long, M. D., A. Levander, and P. M. Shearer (2014), An introduction to the special issue of Earth and Planetary Science Letters on USArray science, *Earth Planet. Sci. Lett.*, *402*, 1–5, doi:10.1016/j.epsl.2014.06.016.
- Ma, S., G. A. Prieto, and G. G. Beroza (2008), Testing community velocity models for southern California using the ambient seismic field, *Bull. Seismol. Soc. Am.*, *98*(6), 2694–2714, doi:10.1785/0120080947.
- Maceira, M., C. Larmat, C. A. Rowe, R. M. Allen, and M. J. Obrebski (2011), Validating seismic imaging methods and 3D seismic velocity models, Abstract S41A-2182 presented at 2011 Fall Meeting, AGU, San Francisco, Calif., Dec.
- Manly, B. F. J. (2007), *Randomization, Bootstrap, and Monte Carlo Methods in Biology*, 3rd ed., Chapman and Hall, London.
- Marquering, H., F. A. Dahlen, and G. Nolet (1999), Three-dimensional sensitivity kernels for finite-frequency traveltimes: The banana-doughnut paradox, *Geophys. J. Int.*, *137*, 805–815.
- Menke, W. (1989), *Geophysical Data Analysis: Discrete Inverse Theory*, Acad. Press, Inc., San Diego, Calif.
- Mercerat, E. D., G. Nolet, and C. Zoroli (2014), Cross-borehole tomography with correlation delay times, *Geophysics*, *79*(1), R1–R12, doi:10.1190/geo2013-0059.1.
- Montelli, R., G. Nolet, F. A. Dahlen, G. Masters, E. R. Engdahl, and S.-H. Hung (2004a), Finite-frequency tomography reveals a variety of plumes in the mantle, *Science*, *303*, 338–343.
- Montelli, R., G. Nolet, G. Masters, F. A. Dahlen, and S.-H. Hung (2004b), Global P and PP traveltime tomography: Rays versus waves, *Geophys. J. Int.*, *158*, 637–654.
- Montelli, R., G. Nolet, F. A. Dahlen, and G. Masters (2006), A catalogue of deep mantle plumes: New results from finite-frequency tomography, *Geochem. Geophys. Geosyst.*, *7*, Q11007, doi:10.1029/2006GC001248.
- Obayashi, M., J. Yoshimitsu, G. Nolet, Y. Fukao, H. Shiobara, H. Sugioka, H. Miyamachi, and Y. Gao (2013), Finite frequency whole mantle P wave tomography: Improvement of subducted slab images, *Geophys. Res. Lett.*, *40*, 5652–5657, doi:10.1002/2013GL057401.
- Obrebski, M., R. M. Allen, M. Xue, and S.-H. Hung (2010), Slab-plume interaction beneath the Pacific Northwest, *Geophys. Res. Lett.*, *37*, L14305, doi:10.1029/2010GL043489.
- Peter, D., L. Boschi, and J. H. Woodhouse (2009), Tomographic resolution of ray and finite-frequency methods: A membrane-wave investigation, *Geophys. J. Int.*, *177*, 624–638, doi:10.1111/j.1365-246X.2009.04098.x.
- Sengupta, M. K., and M. N. Toksöz (1977), Three-dimensional model of seismic velocity variation in the Earth's mantle, *Geophys. Res. Lett.*, *3*, 84–86.
- Showstack, R. (2014), Science is key to decision making, U.S. Secretary of Interior tells Eos, *Eos*, *95*(5), 41–42.
- Spetzler, J., D. Šijačić, and K.-H. Wolf (2007), Application of a linear finite-frequency theory to the time-lapse crosswell tomography in ultrasonic and numerical experiments, *Geophysics*, *72*(6), O19–O27, doi:10.1190/1.2778767.
- VanDecar, J. C., and R. S. Crosson (1990), Determination of teleseismic relative phase arrival times using multi-channel cross-correlation and least squares, *Bull. Seismol. Soc. Am.*, *80*(1), 150–169.
- Wessel, P., and W. H. F. Smith (1991), Free software helps map and display data, *EOS Trans. AGU*, *72*, 441–445.
- Xue, M., and R. M. Allen (2010), Mantle structure beneath the western United States and its implications for convection processes, *J. Geophys. Res.*, *115*, B07303, doi:10.1029/2008JB006079.
- Zoroli, C., E. Debayle, and M. Sambridge (2010), Frequency-dependent effects on global S-wave traveltimes: Wavefront-healing, scattering, and attenuation, *Geophys. J. Int.*, *182*, 1025–1042, doi:10.1111/j.1365-246X.2010.04667.x.